www.sciencemag.org/cgi/content/full/science.1234145/DC1

Supplementary Materials for

Clarifying the Dominant Sources and Mechanisms of Cirrus Cloud Formation

Daniel J. Cziczo,* Karl D. Froyd, Corinna Hoose, Eric J. Jensen, Minghui Diao, Mark A. Zondlo, Jessica B. Smith, Cynthia H. Twohy, Daniel M. Murphy

*Corresponding author. E-mail: djcziczo@mit.edu

Published 9 May 2013 on *Science* Express
DOI: 10.1126/science.1234145

This PDF file includes:

Materials and Methods
Figs. S1 to S4
Tables S1 to S4
Full Reference List

Materials and Methods

Counterflow Virtual Impactor (CVI) and Particle Sampling

The concept of an airborne CVI inlet is that a flow of particle-free gas is directed opposite the motion imparted by the aircraft. This counterflow rejects aerosol particles and small cloud elements (<3-10 μm diameter) from entering the inlet. Large inertia cloud elements (10's to 100's of μm) are able to overcome the counterflow and become incorporated into a sample flow within the inlet *(33)*. The CVI inlet used in these studies was first described by Cziczo et al. *(14)* for the Cirrus Regional Study of Tropical Anvils and Cirrus Layers - Florida Area Cirrus Experiment (CRYSTAL-FACE) flights. The observation that stainless steel inlet material was abraded by ice crystals (see next paragraphs) led to modifications, including coating the inlet with gold to reduce artifact generation and also render the artifacts spectrally distinct. This modified inlet was used during the Costa Rica - AURA Validation Experiment (CRAVE) described by Froyd et al. *(13)*. A second set of modifications was performed for the Mid-latitude Airborne Cirrus Properties Experiment (MACPEX) including a 'folded' flow design and use of Ne as a counterflow gas to improve crystal stopping efficiency and evaporation within the inlet. The CVI inlets are 24 cm in length with a 1.5-2 mm inner diameter (i.d.). The inlets are housed in a 88.5 cm long, 5 cm i.d. duct extending from the NASA WB-57F high altitude research aircraft's nose. In regions with ice crystals the counterflow was initiated so that the unactivated, or interstitial, aerosol was rejected. The low humidity of the heated counterflow was used to remove water from the sampled crystals before characterization by the Particle Analysis by Laser Mass Spectrometry (PALMS) instrument and/or collection of residuals on electron microscope grids. During the Tropical Composition, Cloud and Climate Coupling (TC4) experiment, the National Center for Atmospheric Research CVI inlet *(34,35)* was mounted on the side of the DC-8 aircraft, with the inlet tip 60 cm from the side of the fuselage. This shrouded inlet is constructed internally of stainless steel, with a 0.67 cm i.d. tip, a 7.5 cm long porous tube, a 2.8 cm straight section, and a 13.1 cm long diverging section attached to a 2.22 cm i.d. bend with a 15 cm radius of curvature. Ice crystals were entrained into dry nitrogen gas and the inlet and sample tube were heated to ~50°C to dry the sample before being transmitted to the cabin-mounted PALMS instrument.

In near-cloud areas (i.e., in the absence of ice crystals) particles were sampled directly using the CVI inlet with the counter flow reduced to zero while maintaining the sample flow *(14)* or by switching to a separate forward-facing inlet tube *(13)*, both with residence times of about 70 ms. For comparison purposes we define particles within the same altitude range as detected cirrus crystals as 'near cloud' or 'clear air', with the assumption that these are potential nucleating particles for nearby cirrus. For campaigns where aerosol composition was homogeneous particle spectra were included up to 2 km below detected ice crystals. Short, strong plume perturbations (e.g., smoke plumes, stratospheric intrusions) with composition not representative of campaign averages were removed from the clear sky analysis. Particle statistics are given in Table S1. Although the assumption of nucleation of ice on near cloud aerosol is in most cases reasonable it does not fully consider the more rapid vertical transport of aerosol common in convectively derived (i.e. anvil) cirrus (see text for details).

Single Particle Mass Spectrometry

The NOAA PALMS instrument was used in these studies for particle characterization. PALMS operates by focusing aerosol particles through an aerodynamic inlet into a vacuum region which imparts a size dependent velocity. Light is scattered as particles pass through two 532 nm visible lasers beams set a fixed distance apart. When combined with the size dependent velocity this provides the aerodynamic diameter. A near ultraviolet 193 nm laser is fired at the time of the light scattering event to evaporate the particle and ionize it. A complete mass spectrum is generated from this event. The airborne version of the PALMS instrument is described by Thomson et al. *(36).* The PALMS lower size limit is set by the minimum detectable scattered light which is ~150-250 nm aerodynamic diameter. The upper size limit is set by the aerodynamic inlet at ~3 μm diameter *(13).* Previous studies have shown that atmospheric ice nuclei are found within this range *(37)*. Within this size range there are no known atmospheric particles that are not detectable with the PALMS 193 nm laser ablation methodology and no known detection biases *(13,14, 36-38).*

Single particle mass spectrometry is normally considered a semi-quantitative analysis method *(38)* because the detector signal depends not only on the quantity of substances present but also the efficiency with which they are ionized. The data presented here should be considered indicative of the particle composition and mixing state but not the specific quantities within each particle.

Categorization of Mass Spectra

Individual particles are classified into seven composition classes based on chemical markers in their mass spectra (Table S1). Selection criteria for particle classes were developed using laboratory experiments and flight data during segments with well-defined particle composition such as biomass burning plumes, mineral dust plumes, and the marine boundary layer *(13)*. The particle class is assigned based on the dominant composition or as is descriptive of the particle source, e.g., a mineral dust particle with secondary sulfate and organic material is classified as mineral dust. Particles with unclear spectral signatures or those that do not fit into one of the above categories are classified 'Other'. The large majority of Other particles have signatures that suggest pyridine salts, are organic-rich with unique spectral patterns, or are Sulfate/Organic/Nitrate particles with small, unconfirmed potassium signals possibly indicative of Biomass Burning.

The categorization values provided in Table S1 correspond to the four flight campaigns described here. Values were investigated on a per flight basis and only varied for the homogenous cases described in the text. Sub-flight values were not investigated for two reasons. First, sub-flight differences are not expected because individual flights correspond to single clouds or closely geographically related clouds. Second, we avoid the low statistical significance of sub-flight results which would correspond to fewer than 100 IR.

The presence or absence of surface coatings of sulfate or organic species on mineral dust and metallic aerosol was based on a comparison of the signals from these species from the flight data to an amount of coating known to deactivate dust IN, ~5 – 20% by particle mass *(23)*. Coatings visible in electron microscope images. For these studies coatings with a thickness greater than ~10 nm would have been apparent at the microscope resolution used and, in these cases, was identifiable using electron microscopy/energy dispersive X-ray measurements (see Electron Microscopy section).

Our analysis suggests that >90% of mineral dust and metallic IR had thinner coatings than what has been shown to deactivate dust in lab studies

Mass spectral signatures for biological aerosol particles are defined using PALMS laboratory measurements of bacteria, yeast, and fungal spores. Signals common to all biological organisms were sodium, potassium, and calcium metals internally mixed with phosphate and abundant organic material. These signatures are consistent with other single particle mass spectrometry laboratory studies reported the literature *(27,39)*. In atmospheric samples, PALMS spectra with identifiable phosphate, abundant organic signatures, and one or more of the above metals are selected as biological candidate particles. Candidates containing mineral dust markers such as iron, silicon, aluminum, or zinc were rejected. The same chemical criteria and morphology were used to identify biological candidates using electron microscopy/energy dispersive X-ray measurements in combination with morphological analysis (see Electron Microscopy section). Potassium-containing particles with mineral dust markers and morphology were classified as mineral dust. In no cases were mineral dust particles associated with a possible biological particle such as a bacterium, fungal spore or fragment thereof. Biological candidate particle statistics are summarized in Tables S2 and S3.

CVI Inlet Artifacts

The impaction of cirrus crystals onto aircraft and inlet surfaces generates secondary aerosol particles that are composed of structural materials. When sampling cloud residuals using a CVI inlet, artifact particles generated upstream of the inlet confound measurements of particle size, number, and composition.

Murphy et al. *(40)* and Cziczo et al. *(14)* observed that impaction of cirrus crystals abraded CVI inlet surfaces to generate submicron particles composed of stainless steel. In a similar mechanism, these authors observed that aerosol particles previously captured onto inlet surfaces were resuspended by impaction of cirrus crystals. Several additional mechanisms were identified in the current study, including upstream bounce of artifacts generated downstream of a sampling pickoff inside the inlet, and internal mixtures of real IR with artifact particles resulting from capture by crystal fragments that survive impaction. Artifact spectra were identified from laboratory composition measurements of particles generated from aircraft surfaces (e.g., white paint, aircraft aluminum, and fiberglass) and materials internal to the CVI inlets (gold plating, silicone o-rings, and thermistors). We note that the categorization of IR takes place after elimination of artifacts. For example, gold-containing particles are removed and defined as artifact, never categorized as metallic aerosol.

Artifact generation is a strong function of ice crystal size, aircraft speed, and angle-of-attack. Sampling low altitude ice clouds is particularly artifact-prone since crystal sizes are many factors larger than can be sampled by CVI inlets without impaction. The PALMS and EM composition analyses can reliably differentiate artifacts from real atmospheric IR in most cloud environments. Individual artifact particles were removed based on compositional markers. Cloudy flight segments were screened for artifacts at 1 minute intervals, and those where artifact particles numbered >25% were rejected from the current analysis. In some clouds with large ice crystals, artifact particles are generated at a high rate and constituted 100% of the sample. Overall, artifact particles comprised half or more of all particles sampled inside ice cloud for every flight campaign (see Table S1).

Electron Microscopy

Size, morphology, and elemental composition of ice residual (IR) particles were analyzed from samples collected during MACPEX using the Electron Microscope Ice Residual Impactor (EMIRI). Particles within a 1 liter per minute portion of the CVI inlet sample flow were impacted on Au-coated 200 mesh formvar/carbon grids (Ted Pella, Inc.). Scanning electron microscopy (SEM) and transmission electron microscopy (TEM), combined with energy dispersive X-ray microanalysis, were utilized for sample analysis. Analysis took place at the MIT Center for Materials Science and Engineering Electron Microscope Laboratory. The size distribution of particles analyzed using electron microscopy and PALMS is shown in Fig. S1. This independent technique supports the assertion that PALMS is able to analyze the majority of IR: particles below 200 and 250 nm geometric diameter (an approximate PALMS lower threshold) represent only 5.9 and 11.8% of the total number, respectively.

Water Vapor

Water vapor onboard the NSF Gulfstream-V (G-V) research aircraft was measured by the 25 Hz, open-path Vertical Cavity Surface Emitting Laser (VCSEL) hygrometer *(18)* in the Stratosphere-Troposphere Analyses of Regional Transport (START08) *(41)*, HIAPER Pole-to-Pole Observations (HIPPO) *(42)*,, and Pre-Depression Investigation of Cloud-systems in the Tropics (PREDICT) *(43)* field campaigns. The H_2O measurements were averaged to 1s for consistency with the temperature measurements. A total of 89.9 hours of flight data satisfied the conditions of T < -40 ºC, O_3 < 200 part per billion by volume (ppbv), clear sky, and meteorological Northern Hemisphere latitudes. Temperature was recorded by the NCAR G-V Rosemount temperature probe. Uncertainties in RH_i from the range of -40 to -70 °C were 8 to 10% after combining uncertainties from the VCSEL hygrometer (6%) and temperature probe (±0.5 ºC). The VCSEL hygrometer and temperature probe have precisions of 1% and 0.1 ºC, respectively. In START08, concentrations of ice particles were measured by the HIAPER Small Ice Detector Probe (SID-2H) instrument on the GV aircraft *(44)*. In-cloud regions are defined as the locations where the total ice particle concentrations measured by SID-2H or 2DC instruments are greater than zero during the 1 Hz measurement (~229 m), and the remaining regions are considered to be clear-sky regions. We use the large latitudinal and longitudinal coverage of the VCSEL flights to constrain the relative humidity of the Northern Hemisphere.

Water vapor onboard NASA's WB-57F high altitude research aircraft was measured by the Harvard Water Vapor instrument *(17)*. Ambient pressures and temperatures were acquired by the NASA Ames Meteorological Measurement System (MMS) *(45*), or the NOAA Pressure and Temperature measurement (P/T), depending upon the mission and WB-57 payload configuration. During the CRYSTAL-FACE, CRAVE and MACPEX missions, the data were acquired on the same platform as the PALMS and EMIRI data. During TC4, the data were acquired in the same region, but on a different aircraft. The composite WB-57F RH_i dataset covers more than thirty degrees in temperature, three orders of magnitude in both water vapor and cloud ice water content, and a geographic range from the mid-latitudes to the tropics.

The WB-57F water vapor and temperature data were averaged to 10s for each mission, and selected to be in clear air in the upper troposphere. The combination of the stated uncertainties of the independent water vapor and temperature measurements, ~5%

− 15% (~10% at 5 ppmv) in vapor mixing ratio, and ~±0.5 ºC in temperature, yields an uncertainty of ~±10 − 15% in the clear air RH_i data. The criteria for distinguishing clear air from cloudy air varied by mission in response to changes in payload configuration (e.g., the particle and/or ice water content instrumentation). Similarly, the criteria for identifying upper tropospheric air varied by the geographical location and season of each mission *(46-48)*. The specifics for each mission are provided in Table S4. We include data that was not definitively identified as being in clear air or in cloud due to limitations in the sensitivity of the particle sensors or total water measurements because they are expected to capture the RH_i transition at the cloud boundaries *(49)*.

Three factors dictate the distribution of RH_i in clear air: ambient water vapor concentrations, ambient temperature, and the threshold for ice nucleation, RH_{nuc}, which functions as a nominal upper bound to RH_i in clear air. The high end of the clear air RH_i distribution can be truncated by cirrus formation (i.e., when RH_i reaches RH_{nuc}) and this cutoff RH_i is often used to infer the threshold saturation required for ice nucleation, and thus to identify the dominant mode of ice nucleation *(15,50)*. The fact that clear air RH_i values rarely exceed typical heterogeneous nucleation levels supports the conclusion that heterogeneous nucleation appears to be the dominant mode for cirrus formation in this data set.

It is noteworthy that is that in situ measurements of clear air RH_i at or near most cloud boundaries rarely coincide with regions of active nucleation and/or cloud formation, and thus seldom provide an actual measure of RH_{nuc}. Previous studies targeted active nucleation in cirrus cloud tops and wave clouds in order to constrain RH_{nuc} *(51,52)*. This was not possible in the current study due to complex cirrus generated from convective anvils and detrained into either supersaturated or under-saturated ambient air.

In addition to the two cases of homogeneous nucleation described in the text we note IN abundance, regional, seasonal and annual variability also play a role in freezing mode. Data acquired during the MIDCIX mission are compared to MACPEX in Fig. S2. During MIDCIX clear air RH_i observations occasionally approached levels consistent with homogeneous freezing, ~155%, whereas during MACPEX clear air RH_i rarely exceeded 120%. Figure S2 (panel C) shows normalized frequency distributions for the clear RH_i data from each mission. Note that ice residual measurements were not made during MidCIX.

Ice Crystal Number Density

Recently, in situ measurements of ice crystal number density have been shown to have been affected by artifacts associated with shattering, and thus overcounting *(53-55)*. The presence of potential artifacts precludes an accurate comparison to our particle and RH_i data during all airborne campaigns. Recently redesigned instrumentation allows for comparison to the data of Jensen et al. using a 2-Dimensional Stereo (2D-S) and Video Ice Particle Sampler (VIPS) probe deployed during the MACPEX study *(17)*. Jensen et al. show that high crystal number densities consistent with homogeneous freezing are rare, exceeding 1000 per liter in less than 1% of cirrus, and exceeding 200 per liter in only about 10% of cirrus. However, it is worth noting that cloud processes such as entrainment and differential sedimentation will reduce ice concentrations as cirrus evolve. As a result, regions in cirrus with high ice concentrations produced by homogeneous freezing are likely to be transient but nevertheless observable by statistical cloud sampling. Moreover, a correlation between high ice number concentration and

homogenous freezing inferred by IR composition was not apparent in these data. Much of the cloud system will have lower ice concentrations that could be interpreted as consistent with heterogeneous freezing.

Field Studies

CRYSTAL-FACE

The Cirrus Regional Study of Tropical Anvils and Cirrus Layers - Florida Area Cirrus Experiment based in Key West, FL, USA during July, 2002. The IR and RH_i data were collected aboard the NASA WB-57F. This was a multi-agency mission and included six research aircraft. The major objective relating to this study was determination of the formation conditions and evolution of anvil cirrus to be used as input for climate models. All IR measurements were taken within convective anvil cirrus at altitudes of 5-15 km with the exception of one flight through in-situ synoptic cirrus at 14.5 km. Convective inflow regions were mostly marine environments with minor contributions from local continental and marine with Saharan dust layer influence. A complete list of residual and near-cloud aerosol particle number is provided in Table S1. These data have been previously considered by Cziczo et al. *(14)* The study website can be found at: http://www.espo.nasa.gov/crystalface/.

CRAVE

The Costa Rica AURA Validation Experiment was conducted from San Jose, Costa Rica during January and February, 2006. The IR and RH_i data were collected aboard the NASA WB-57F. CRAVE was designed to explore the tropical upper troposphere to provide information for comparison to satellite observations. All IR measurements were taken within convective anvil cirrus at 6-16 km. Convective inflow regions were an even mixture of continental, marine, and coastal environments. IR measurements within in-situ, subvisible cirrus at tropopause levels (17 km) from Froyd et al. *(13)* are not included in this study. A complete list of residual and near-cloud particle number is provided in Table S1. The data presented here have not been previously considered. The study website can be found at: http://www.espo.nasa.gov/ave-costarica2/.

TC4

The Tropical Composition, Cloud and Climate Coupling aircraft campaign was conducted from San Jose, Costa Rica during July and August, 2007. The IR data were collected aboard the NASA DC-8, and the RH_i data aboard the NASA WB-57F. The objective of TC4 was to investigate structure, properties and processes of aerosol particles and clouds in the tropical Eastern Pacific. Comparisons were used for validation of the A-train satellite and observations were used to provide information on spatial and temporal cloud variability. All IR measurements were taken within convective anvil cirrus at 8-13 km. Convective inflow regions were predominantly marine and coastal environments with a minor continental contribution. A complete list of residual and near-cloud particle number is provided in Table S1. The data presented here have not been previously considered. The study website can be found at: http://www.espo.nasa.gov/tc4/.

MACPEX

The Mid-latitude Airborne Cirrus Properties Experiment was based in Houston, TX, USA during March and April, 2012. The IR and RH_i data were collected aboard the NASA WB-57F. The MACPEX study sought to investigate the formation and properties of cirrus clouds and their impact on the Earth's radiative budget. Flights predominantly focused on central North America. IR measurements were taken within both synoptic and

convective anvil cirrus at 6-13 km. For the convective systems, inflow regions were exclusively continental. A complete list of residual and near-cloud aerosol particle number is provided in Table S1. The data presented here have not been previously considered. The study website can be found at: http://www.espo.nasa.gov/macpex/.

MidCiX

The Middle Latitude Cirrus Experiment was conducted from Houston, TX, USA during April and May, 2004. The RH_i data were collected aboard the NASA WB-57F. The MidCIX study sought to investigate the formation and properties of cirrus clouds and their impact on the Earth's radiative budget. Flights predominantly focused on central North America. The data presented here have not been previously considered. The study website can be found at: http://meteo04.chpc.utah.edu/cgi-bin/midcix/midcix.cgi.

START08

The United States National Science Foundation (NSF) Stratosphere-Troposphere Analyses of Regional Transport11 aircraft campaign took place in May-June 2008 based out of Broomfield, Colorado. START08 focused on extratropical stratosphere-troposphere processes and dynamics *(41)*. The VCSEL recorded 61 total flight hours of data with T < -40 ºC, of which 26.6 hours also satisfied O_3 < 200 ppbv and clear sky.

HIPPO

The HIAPER Pole-to-Pole Observations12 campaign took place in five deployments from January 2009 to September 2011 from 87ºN north of Alaska through the central Pacific to New Zealand to 67ºS. HIPPO examined the vertical and meridional distribution of greenhouse gases as a function of season from the Antarctic to the Arctic *(42)*. A total of 155 flight hours were at T < -40ºC. The subset of data within Fig. 2 (Panel B; north of 8ºN, clear sky, T < -40ºC, O_3 < 200 ppbv) was 39.5 hours.

PREDICT

The Pre-Depression Investigation of Cloud-systems in the Tropics (PREDICT) campaign took place in August-September 2010 based out of St. Croix, U.S. Virgin Islands with 92 hours of flight time for the VCSEL. PREDICT investigated the dynamics of how tropical cycle disturbances turn into tropical cyclones *(43)*. A total of 23.8 hours satisfied the criteria of clear sky, T < -40ºC, and O_3 < 200 ppbv. All data were in the meteorological Northern Hemisphere.

Model-based IN Estimates

Particle concentrations

Bacteria, fungal spores and pollen have been implemented into the CAM-Oslo model with simple emission functions depending on ecosystem type, leaf area index and specific humidity *(32)*. In this study, the bioaerosol concentrations were simulated with CAM-Oslo at a resolution of 2.8°x2.8° with 26 vertical levels. For mineral dust and EC from fossil fuel combustion surface area concentrations were calculated with a modified version of CAM4-Oslo in a resolution of 1.875°x2.5°, also with 26 vertical levels *(31)*. Emissions from fossil fuel combustion, often termed 'soot' as opposed to EC due to complex mixing with organic components, were provided by the inventory by Lamarque et al. *(56)* for the year 2000, while mineral dust emissions from desert areas were based on Dentener et al. *(57)*. Surface area concentrations were summed over both uncoated and coated dust and EC particles. The IN calculations are based on multi-annual average concentrations for 0 to 60°N, 210 to 300°E and 500 to 200hPa (covering roughly the area of the flights presented in this article) from these two model simulations. We note that

CAM4-Oslo has one of the highest EC burdens among the models analyzed in the AEROCOM Phase II global model intercomparison *(58)* but that this is likely due to the high biomass burning emissions in the year 2006 inventory. This inventory was not used in this work. Kirkevåg et al. *(31)* show that surface level mass concentrations of both EC and mineral dust tend to be underestimated in CAM4-Oslo.

IN activity

Ice nucleation active surface site (INAS) density for each IN type was determined from IN concentrations and particle surface area as a function of temperature and RHi *(9,59)*. In the limit of small activated fractions, which is valid for all particles investigated except the mineral dust coarse mode, the number of IN is directly given by the product of the INAS density with the aerosol particle surface area. The INAS density was derived from a large number of laboratory experiments in the immersion freezing and deposition nucleation modes *(9)*. Data were parameterized by fits published in the literature and derived for this study, Fig. S3 and S4 *(60-62)*. It should be noted that the INAS densities derived from laboratory measurements often span several orders of magnitude. For mineral dust, model results do not account for the possible suppression of deposition nucleation on coated particles. For EC, where laboratory results are inconsistent (for both immersion and deposition freezing), we derive and present upper and lower limits of the INAS density. For bacteria, the fit refers to the most active cells with the range of less active particles indicated by the shaded area. For fungal spores, the fit is based on measurements with Cladosporium spores by Iannone et al. *(63)*. While some authors report that other fungi can initiate ice nucleation at higher temperatures, the data is incomplete and was not used to derive INAS densities.

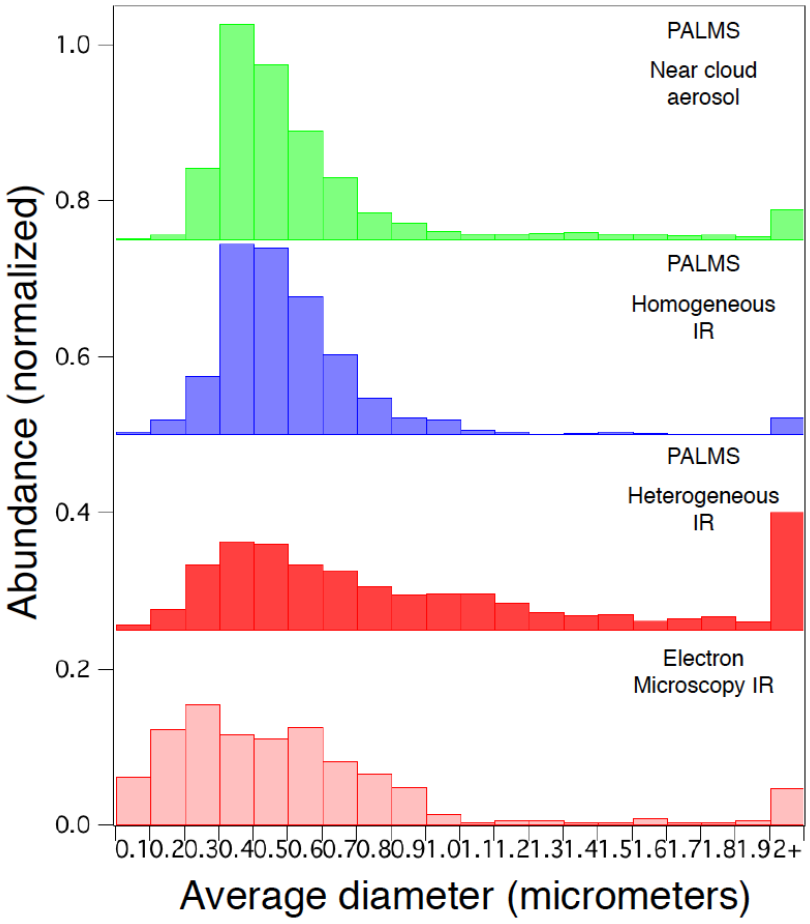

Fig. S1.

Normalized histogram of IR and clear air aerosol size. Geometric diameter of IR analyzed using electron microscopy during MACPEX (light red), and aerodynamic diameter from PALMS for all mission heterogeneous (dark red) and homogeneous (blue) IR and near cloud aerosol (green) analyzed using PALMS. Particles are binned in 0.1 micrometer groups with all particles greater than 2 micrometers diameter placed in the uppermost size bin. Particle statistics and chemical composition are given in Table S1. Comparison with the EM size distribution confirms that IR particles too small for PALMS to detect (<200 nm) are not a substantial fraction of the IR.

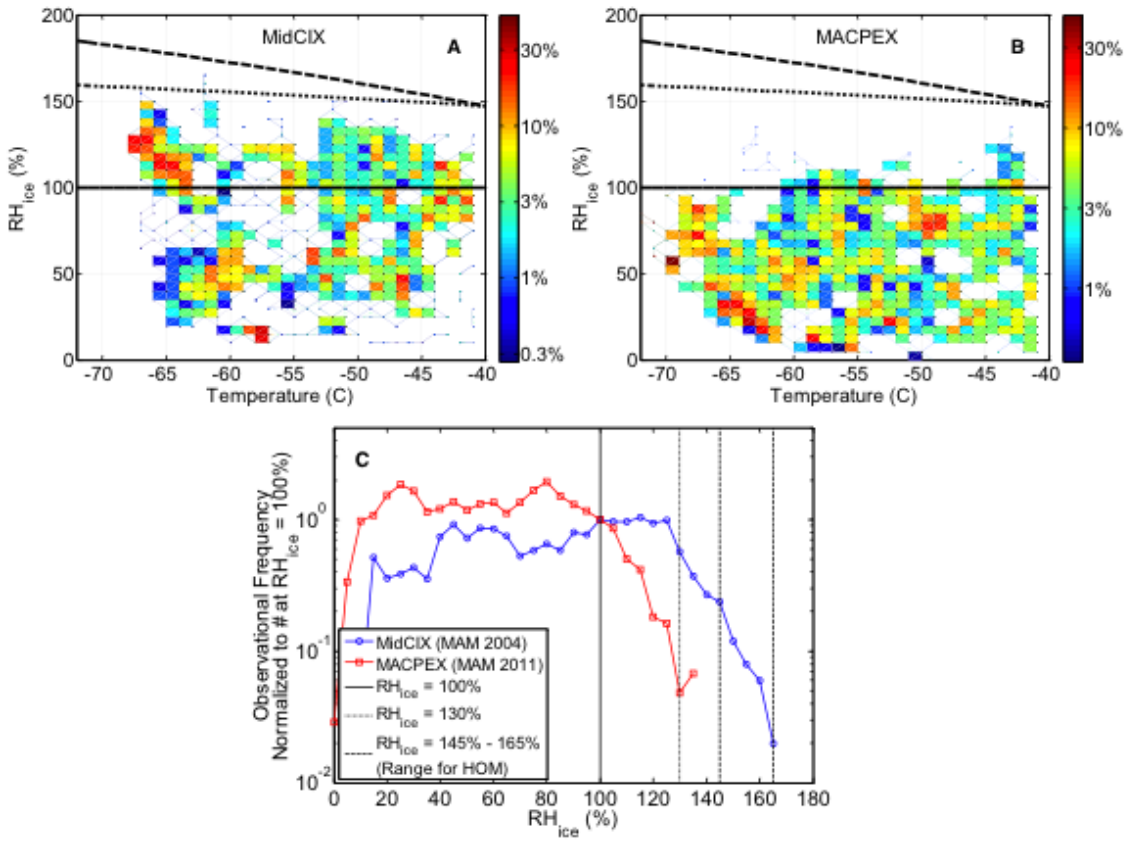

Fig. S2

The distribution of upper tropospheric clear air relative humidity with respect to ice (RHi) as a function of temperature. The color-coding corresponds to the frequency of observations at a specific RHi in a 1° C range. The solid and thick dashed lines indicate ice and water saturation, respectively. The thin dashed lines denote the onset of homogeneous ice nucleation and water saturation. (A) Data collected during MidCIX. (B) Data collected during MACPEX. (C) Histogram of both flight data sets. The MidCIX data exhibit a consistently higher RHi than during MACPEX with more frequent occurrence of RHi approaching the homogeneous freezing threshold. Note that ice residual measurements were not made during MidCIX.

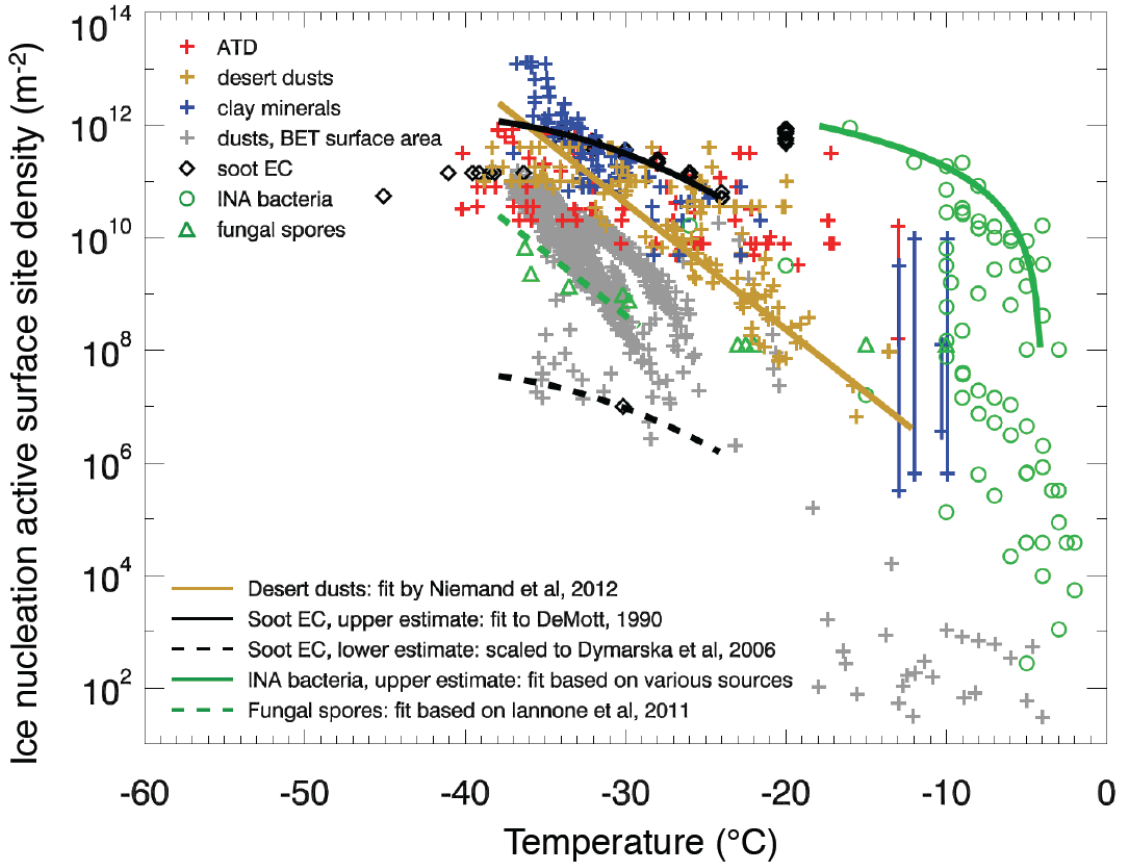

Fig. S3

Ice nucleation active surface site density versus temperature for various aerosol particles in the immersion and condensation freezing mode. The symbols refer to a compilation of laboratory data, with estimates assuming spherical particles *(9)*. The lines indicate fits provided by Niemand et al. *(60)* for desert dusts, by Murray et al. *(61)* for relatively ice nucleation active EC (based on the acetylene burner data by DeMott *(62)*), and estimates for fungal spores (based on Cladosporium data by Iannone et al. *(63)* assuming the slope of Niemand et al. *(60)*), for EC which is inactive in the condensation freezing mode (based on the upper limit by Dymarska et al. *(25)* and assuming the slope of Murray et al. *(61)*), and for the most active ice nucleation active (INA) biological materials *(64-67)*. Figure adapted from Hoose and Möhler *(9)*. Estimates for dusts using BET surface areas are included for comparison.

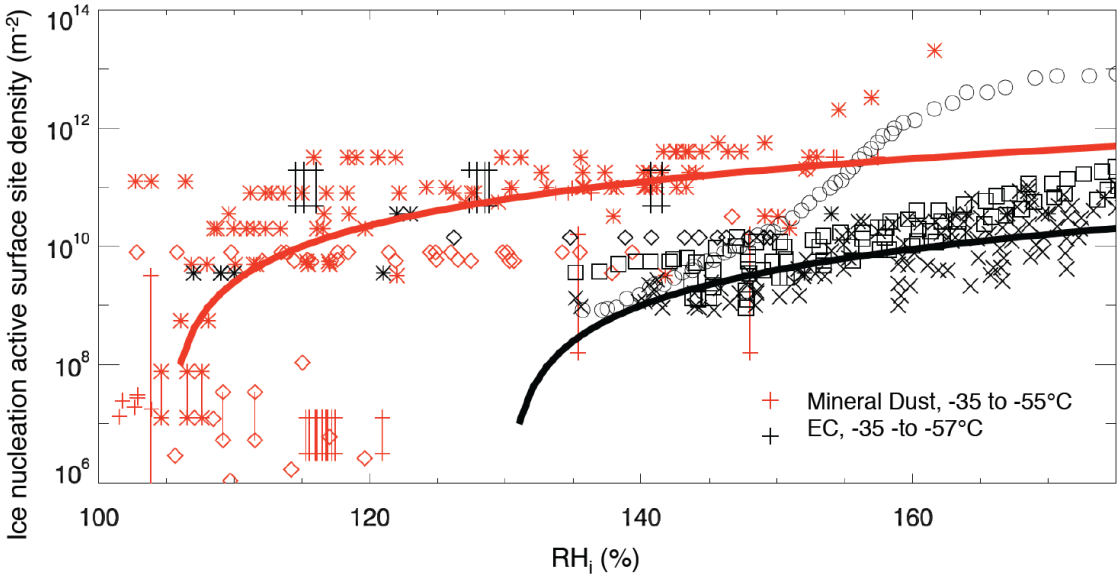

Fig. S4

Ice nucleation active surface site densities versus relative humidity with respect to ice for mineral dust and EC in the deposition mode. The symbols refer to a compilation of laboratory data. Estimates assume spherical particles *(9)*. The mineral dust data are based on 19 studies with Arizona test dust, kaolinite and desert dusts as listed in Hoose and Möhler *(9)*. The black symbols refer to graphite spark generator emissions (crosses, Möhler et al. *(66)* and diamonds, Kanji et al. *(69)*), CAST soot with variable organic carbon content (stars, Crawford et al. *(70)*), and soot from different combustion sources (others, Koehler et al. *(71)*). The red line is a fit for mineral dust of average IN activity. The red line also corresponds to the highest estimate of soot IN activity. The black line represents the lower estimate for soot IN activity.

	MACPEX 2011				TC4 2007		CRAVE 2006		CRYSTAL-FACE 2002		
Category	**Cirrus IR (Hom)**	**Cirrus IR (Het)**	**Cirrus IR (Het)[a]**	**Aerosol**	**Cirrus IR (Het)**	**Aerosol**	**Cirrus IR (Het)**	**Aerosol**	**Cirrus IR (Hom)**	**Cirrus IR (Het)**	**Aerosol**
Sulfate/Organic /Nitrate	81 38%	11 9%	67 15%	2467 39%	70 16%	3889 76%	65 14%	2112 82%	138 55%	97 15%	446 24%
Biomass Burning	83 39%	12 10%	32 7%	2603 42%	9 2%	936 18%	9 2%	329 13%	81 32%	22 3%	1337 73%
Elemental Carbon	0 0%	0 0%	2 <1%	38 1%	0 0%	10 <1%	7 1%	9 <1%	1 0%	2 <1%	4 <1%
Sea Salt	1 <1%	3 3%	17 4%	42 1%	135 31%	19 <1%	11 2%	11 <1%	4 2%	127 19%	5 <1%
Mineral Dust and Metallic	21 10%	65 56%	251 58%	681 11%	221 50%	116 2%	370 79%	97 4%	25 10%	403 62%	40 2%
Oil Combustion	3 1%	0 0%	--	35 1%	0 0%	27 1%	4 1%	4 <1%	0 0%	0 0%	3 <1%
Other	25 12%	25 22%	64 15%	403 6%	3 1%	116 2%	1 <1%	10 <1%	2 1%	1 <1%	1 <1%
Total Classified	214 87%	116 31%	433 74%	6269 100%	438 17%	5113 100%	467 51%	2572 100%	251 40%	652 9%	1836 100%
Total Artifact[b]	31 13%	260 69%	149 26%	--	2072 83%	--	443 49%	--	376 60%	6701 91%	--

[a] From offline EMIRI analysis. All other points from PALMS.
[b] Artifact particles that were rejected from the analysis.

Table S1.

Number and percent of analyzed ice residuals (IR) and background aerosol particles classified into compositional categories.

	MACPEX 2011			TC4 2007		CRAVE 2006		CRYSTAL-FACE 2002	
Signature	**Cirrus IR**	**Cirrus IR[a]**	**Aerosol**	**Cirrus IR**	**Aerosol**	**Cirrus IR**	**Aerosol**	**Cirrus IR**	**Aerosol**
Phosphate with crustal metals	1 0.3%	3 1.1%	3 0.05%	2 0.5%	0	10 2.1%	1 0.04%	8 0.9%	2 0.1%
Possible phosphate, very low intensity	1 0.3%	--	0	0	2 0.04%	0	0	0	3 0.2%
Potassium or calcium phosphate	0	1 0.2%	1 0.02%	0	0	0	0	0	0
Phosphate, high intensity in Sulfate/Organic /Nitrate particle	0	1 1.5%	3 0.05%	0	1 0.02%	1 0.2%	0	1 0.1%	0
Total particles analyzed	330	433	6269	438	5113	467	2572	903	1836
Total with phosphate	2 0.6%	5 1.2%	7 0.1%	2 0.5%	3 0.06%	11 2.4%	1 0.04%	9 1.0%	5 0.3%
Total Biocandidates	0	1 0.2%	4 0.06%	0	1 0.02%	1 0.2%	0	1 0.1%	0

[a] From offline EMIRI analysis. All other points from PALMS.

Table S2.

Candidate biological particle analysis using positive ion mass spectra and electron microscopy.

	MACPEX 2011		TC4 2007		CRAVE 2006		CRYSTAL-FACE 2002	
Signature	**Cirrus IR**	**Aerosol**	**Cirrus IR**	**Aerosol**	**Cirrus IR**	**Aerosol**	**Cirrus IR**	**Aerosol**
Phosphate with crustal metals	11 3.5%	18 0.4%	19 0.8%	3 0.06%	7 1.9%	1 0.05%	40 1.0%	1 0.04%
Phosphate mixed with chloride and without metals	4 1.3%	7 0.2%	8 0.3%	0	2 0.5%	0	1 0.02%	0
Phosphate in Elemental Carbon particle	2 0.6%	0	0	0	0	0	0	0
Phosphate in Sulfate/Organic /Nitrate particle	0	2 0.04%	0	2 0.04%	0	0	0	0
Total particles analyzed	314	4482	2350	4884	364	2167	4151	2249
Total with phosphate	17 5.4%	27 0.6%	27 1.1%	5 0.1%	9 2.5%	1 0.05%	41 1.0%	1 0.04%
Total Biocandidates	6 1.9%	9 0.2%	8 0.3%	2 0.04%	2 0.5%	0	1 0.02%	0

Table S3.

Candidate biological particle analysis using negative ion mass spectra. IR include an unknown number of artifact particles which are not reliably identified in negative ion spectra.

Mission (# Flights)	Season, Region	Potential Temperature	Clear (& Uncertain) Air Criteria
CRYSTAL-FACE (11)	Summer, Sub-tropical	335 – 380 K	FSSP[a] ND < 3 L^{-1}
CRAVE (6)	NH Winter, Tropics	340 – 410 K	CPI[b] ND = NaN, or CPI ND < 1 L^{-1}
TC4 (7)	NH Summer, Tropical	340 – 410 K	CPI ND ≤ 0.1 L^{-1} prior to 20070809 CLH[c] ICE < 1 ppmv for 20070809+
MACPEX (11)	Spring, Mid-latitude	325 – 355 K	CLH ICE = NaN, or (FISH[d] TW – HWV) ≤ 30% of HWV
MidCIX (8)	Spring, Mid-latitude	325 – 355 K	FSSP ND < 3 L^{-1}

[a] FSSP ND: Particle number density measured by the SPP-100 optical particle counter from Stratton Park Engineering Company, Inc., (SPEC).
[b] CPI ND: Particle number density measured in situ by the Cloud Particle Imager (*46*).
[c] CLH: University of Colorado Laser Hygrometer (CLH) measures enhanced total water, and provides a derived cloud ice water content product (*47*).
[d] FISH TW: Fast In Situ Hygrometer (FISH) measures enhanced total water (*48*).

Table S4.

Criteria for upper tropospheric clear air data selection by mission with potential temperature used to define the upper tropospheric region shown for each mission. Changes in geographic region and season, noted in the table, necessitated mission-specific definitions. Also shown are the criteria for the determination of cloud-free air.

References and Notes

1. S. Solomon, Ed., *Climate Change 2007: The Physical Science Basis. Contribution of Working Group I to the Fourth Assessment Report of the Intergovernmental Panel on Climate Change* (Cambridge Univ. Press, Cambridge, 2007).

2. D. K. Lynch, K. Sassen, D. C. Starr, G. Stephens, Eds., *Cirrus* (Oxford Univ. Press, New York, 2002).

3. U. Lohmann, A glaciation indirect aerosol effect caused by soot aerosols. *Geophys. Res. Lett.* **29**, 11-1 (2002). doi:10.1029/2001GL014357

4. H. R. Pruppacher, J. D. Klett, *Microphysics of Clouds and Precipitation* (Kluwer Academic, Dordrecht, ed. 2, 1997), pp. 309–354.

5. T. Koop, B. P. Luo, A. Tsias, T. Peter, Water activity as the determinant for homogeneous ice nucleation in aqueous solutions. *Nature* **406**, 611 (2000). doi:10.1038/35020537 Medline

6. D. M. Murphy, D. S. Thomson, M. J. Mahoney, In situ measurements of organics, meteoritic material, mercury, and other elements in aerosols at 5 to 19 kilometers. *Science* **282**, 1664 (1998). doi:10.1126/science.282.5394.1664

7. A. Gettelman, X. Liu, D. Barahona, U. Lohmann, C. Chen, Climate impacts of ice nucleation. *J. Geophys. Res.* **117**, D20201 (2012). doi:10.1029/2012JD017950

8. P. J. DeMott *et al*., Measurements of the concentration and composition of nuclei for cirrus formation. *Proc. Natl. Acad. Sci. U.S.A.* **100**, 14655 (2003). doi:10.1073/pnas.2532677100 Medline

9. C. Hoose, O. Möhler, Heterogeneous ice nucleation on atmospheric aerosols: A review of results from laboratory experiments. *Atmos. Chem. Phys.* **12**, 9817 (2012). doi:10.5194/acp-12-9817-2012

10. B. J. Murray *et al*., Heterogeneous nucleation of ice particles on glassy aerosols under cirrus conditions. *Nat. Geosci.* **3**, 233 (2010). doi:10.1038/ngeo817

11. J. P. D. Abbatt *et al*., Solid ammonium sulfate aerosols as ice nuclei: A pathway for cirrus cloud formation. *Science* **313**, 1770 (2006). doi:10.1126/science.1129726

12. Materials and methods are available as supplementary materials on *Science* Online.

13. K. D. Froyd, D. M. Murphy, P. Lawson, D. Baumgardner, R. Herman, Aerosols that form subvisible cirrus at the tropical tropopause. *Atmos. Chem. Phys.* **10**, 209 (2010). doi:10.5194/acp-10-209-2010

14. D. J. Cziczo, D. M. Murphy, P. K. Hudson, D. S. Thomson, Single particle measurements of the chemical composition of cirrus ice residue during CRYSTAL-FACE. *J. Geophys. Res.* **109**, D04201 (2004). doi:10.1029/2003JD004032

15. A. J. Heymsfield, L. M. Miloshevich, C. Twohy, G. Sachse, S. Oltmans, Upper-tropospheric relative humidity observations and implications for cirrus ice nucleation. *Geophys. Res. Lett.* **25**, 1343 (1998). doi:10.1029/98GL01089

16. M. Krämer *et al*., Ice supersaturations and cirrus cloud crystal numbers. *Atmos. Chem. Phys.* **9**, 3505 (2009). doi:10.5194/acp-9-3505-2009

17. E. M. Weinstock *et al*., New fast-response photofragment fluorescence hygrometer for use on the NASA ER-2 and the Perseus remotely piloted aircraft. *Rev. Sci. Instrum.* **65**, 3544 (1994). doi:10.1063/1.1144536

18. M. A. Zondlo, M. E. Paige, S. M. Massick, J. A. Silver, Development, flight performance, and calibrations of the NSF Gulfstream-V vertical cavity surface emitting laser (VCSEL) hygrometer. *J. Geophys. Res.* **115**, D20309 (2010). doi:10.1029/2010JD014445

19. E. J. Jensen, P. Leonhard, P. Lawson, Using statistical comparisons between simulations and observations to understand physical processes controlling midlatitude cirrus ice size distributions, paper presented at the 16th International Conference on Clouds and Precipitation, Leipzig, Germany, 31 July 2012.

20. A. Wiacek, T. Peter, U. Lohmann, The potential influence of Asian and African mineral dust on ice, mixed-phase and liquid water clouds. *Atmos. Chem. Phys.* **10**, 8649 (2010). doi:10.5194/acp-10-8649-2010

21. M. Ebert *et al*., Chemical composition and mixing-state of ice residuals sampled within mixed phase clouds. *Atmos. Chem. Phys.* **11**, 2805 (2011). doi:10.5194/acp-11-2805-2011

22. A. C. Targino, R. Krejci, K. J. Noone, P. Glantz, Single particle analysis of ice crystal residuals observed in orographic wave clouds over Scandinavia during INTACC experiment. *Atmos. Chem. Phys.* **6**, 1977 (2006). doi:10.5194/acp-6-1977-2006

23. D. J. Cziczo *et al*., Deactivation of ice nuclei due to atmospherically relevant surface coatings. *Environ. Res. Lett.* **4**, 044013 (2009). doi:10.1088/1748-9326/4/4/044013

24. T. Kojima, P. R. Buseck, Y. Iwasaka, A. Matsuki, D. Trochkine, Sulfate-coated dust particles in the free troposphere over Japan. *Atmos. Res.* **82**, 698 (2006). doi:10.1016/j.atmosres.2006.02.024

25. M. Dymarska *et al*., Deposition ice nucleation on soot at temperatures relevant for the lower troposphere. *J. Geophys. Res.* **111**, D04204 (2006). doi:10.1029/2005JD006627

26. O. Möhler, P. J. DeMott, G. Vali, Z. Levin, Microbiology and atmospheric processes: The role of biological particles in cloud physics. *Biogeosciences* **4**, 1059 (2007). doi:10.5194/bg-4-1059-2007

27. K. A. Pratt *et al*., In-situ detection of biological particles in high altitude dust-influenced ice clouds. *Nat. Geosci.* **2**, (2009). doi:10.1038/ngeo521

28. C. H. Twohy, M. R. Poellot, Chemical characteristics of ice residual nuclei in anvil cirrus clouds: Implications for ice formation processes. *Atmos. Chem. Phys.* **5**, 2289 (2005). doi:10.5194/acp-5-2289-2005

29. D. J. Cziczo *et al*., Inadvertent climate modification due to anthropogenic lead. *Nat. Geosci.* **2**, 333 (2009). doi:10.1038/ngeo499

30. D. M. Murphy *et al*., Distribution of lead in single atmospheric particles. *Atmos. Chem. Phys.* **7**, 3195 (2007). doi:10.5194/acp-7-3195-2007

31. A. Kirkevåg *et al*., Aerosol-climate interactions in the Norwegian Earth System Model – NorESM. *Geosci. Model Dev.* **6**, 207 (2013). doi:10.5194/gmd-6-207-2013

32. C. Hoose, J. E. Kristjánsson, S. M. Burrows, How important is biological ice nucleation in clouds on a global scale? *Environ. Res. Lett.* **5**, 024009 (2010). doi:10.1088/1748-9326/5/2/024009

33. J. A. Ogren, J. Heintzenberg, R. J. Charlson, In situ sampling of clouds with a droplet to aerosol converter. *Geophys. Res. Lett.* **12**, 121 (1985). doi:10.1029/GL012i003p00121

34. C. H. Twohy, J. W. Strapp, M. Wendisch, Performance of a counterflow virtual impactor in the NASA Icing Research Tunnel. *J. Atmos. Ocean. Technol.* **20**, 781 (2003). doi:10.1175/1520-0426(2003)020<0781:POACVI>2.0.CO;2

35. C. S. McNaughton *et al*., Results from the DC-8 Inlet Characterization Experiment (DICE): Airborne versus surface sampling of mineral dust and sea salt aerosols. *Aerosol Sci. Technol.* **41**, 136 (2007). doi:10.1080/02786820601118406

36. D. S. Thomson, M. E. Schein, D. M. Murphy, Particle analysis by laser mass spectrometry WB-57F instrument overview. *Aerosp. Sci. Technol.* **33**, 153 (2000). doi:10.1080/027868200410903

37. D. J. Cziczo *et al*., Particle analysis by laser mass spectrometry (PALMS) studies of ice nuclei and other low number density particles. *Inter. J. Mass Spec.* **258**, 21 (2006). doi:10.1016/j.ijms.2006.05.013

38. D. M. Murphy, The design of single particle laser mass spectrometers. *Mass Spectrom. Rev.* **26**, 150 (2007). doi:10.1002/mas.20113 Medline

39. D. P. Fergenson *et al*., Reagentless detection and classification of individual bioaerosol particles in seconds. *Anal. Chem.* **76**, 373 (2004). doi:10.1021/ac034467e Medline

40. D. M. Murphy *et al*., Particle generation and resuspension in aircraft inlets when flying in clouds. *Aerosol Sci. Technol.* **38**, 401 (2004). doi:10.1080/02786820490443094

41. L. L. Pan *et al*., The Stratosphere-troposphere analyses of regional transport 2008 (START08) experiment. *Bull. Am. Meteorol. Soc.* **91**, 327 (2010). doi:10.1175/2009BAMS2865.1

42. S. C. Wofsy *et al*., HIAPER Pole-to-Pole Observations (HIPPO): Fine grained, global scale measurements for determining rates for transport, surface emissions, and removal of climatically important atmospheric gases and aerosols. *Philos Trans. R. Soc. London Ser. A* **369**, 2073 (2011). doi:10.1098/rsta.2010.0313

43. M. T. Montgomery *et al*., The Pre-Depression Investigation of Cloud-Systems in the Tropics (PREDICT) experiment: Scientific basis, new analysis tools, and some first results. *Bull. Am. Meteorol. Soc.* **93**, 153 (2012). doi:10.1175/BAMS-D-11-00046.1

44. R. Cotton *et al*., The ability of the Small Ice Detector (SID-2) to characterize cloud particle and aerosol morphologies obtained during flights of the FAAM BAe-146 research aircraft. *J. Atmos. Ocean. Technol.* **27**, 290 (2010). doi:10.1175/2009JTECHA1282.1

45. S. G. Scott, T. P. Bui, K. R. Chan, S. W. Bowen, The meteorological measurement system on the NASA ER-2 aircraft. *J. Atmos. Ocean. Technol.* **7**, 525 (1990). doi:10.1175/1520-0426(1990)007<0525:TMMSOT>2.0.CO;2

46. R. P. Lawson, B. A. Baker, C. G. Schmitt, T. L. Jensen, An overview of microphysical properties of Arctic clouds observed in May and July during FIRE ACE. *J. Geophys. Res.* **106**, 14989 (2001). doi:10.1029/2000JD900789

47. S. Davis, A. G. Hallar, L. Avallone, W. Engblom, Measurement of total water with a tunable diode laser hygrometer: Inlet analysis, calibration procedure, and ice water content determination. *J. Atmos. Ocean. Technol.* **24**, 463 (2007). doi:10.1175/JTECH1975.1

48. M. Zöger *et al*., Fast in situ stratospheric hygrometers: A new family of balloon-borne and airborne Lyman α photofragment fluorescence hygrometers. *J. Geophys. Res.* **104**, 1807 (1999). doi:10.1029/1998JD100025

49. J. B. Smith, thesis, Harvard University (2012).

50. W. Haag *et al*., Freezing thresholds and cirrus cloud formation mechanisms inferred from in situ measurements of relative humidity. *Atmos. Chem. Phys.* **3**, 1791 (2003). doi:10.5194/acp-3-1791-2003

51. J. M. Comstock, T. P. Ackerman, D. D. Turner, Evidence of high ice supersaturation in cirrus clouds using ARM Raman lidar measurements. *Geophys. Res. Lett.* **31**, L11106 (2004). doi:10.1029/2004GL019705

52. A. J. Heymsfield, L. M. Miloshevich, Relative humidity and temperature influences on cirrus formation and evolution: Observations from wave clouds and FIRE II. *J. Atmos. Sci.* **52**, 4302 (1995). doi:10.1175/1520-0469(1995)052<4302:RHATIO>2.0.CO;2

53. E. J. Jensen *et al*., On the importance of small ice crystals in tropical anvil cirrus. *Atmos. Chem. Phys.* **9**, 5519 (2009). doi:10.5194/acp-9-5519-2009

54. A. V. Korolev *et al*., Small ice particles in tropospheric clouds: Fact or artifact? *Bull. Am. Meteorol. Soc.* **92**, 967 (2011). doi:10.1175/2010BAMS3141.1

55. G. M. McFarquhar *et al*., The importance of small ice crystals to cirrus properties: Observations from the Tropical Warm Pool International cloud Experiment (TWP-ICE). *Geophys. Res. Lett.* **57**, L13803 (2007). doi:10.1029/2007GL029865

56. J.-F. Lamarque *et al*., Historical (1850–2000) gridded anthropogenic and biomass burning emissions of reactive gases and aerosols: methodology and application. *Atmos. Chem. Phys.* **10**, 7017 (2010). doi:10.5194/acp-10-7017-2010

57. F. Dentener *et al*., Emissions of primary aerosol and precursor gases in the years 2000 and 1750 prescribed data-sets for AeroCom. *Atmos. Chem. Phys.* **6**, 4321 (2006). doi:10.5194/acp-6-4321-2006

58. G. Myhre *et al*., Radiative forcing of the direct aerosol effect from AEROCOM phase II simulations. *Atmos. Chem. Phys.* **13**, 1853 (2013). doi:10.5194/acp-13-1853-2013

59. P. J. Connolly *et al*., Studies of heterogeneous freezing by three different desert dust samples. *Atmos. Chem. Phys.* **9**, 2805 (2009). doi:10.5194/acp-9-2805-2009

60. M. Niemand *et al*., A particle-surface-area-based parameterization of immersion freezing on desert dust particles. *J. Atmos. Sci.* **69**, 3077 (2012). doi:10.1175/JAS-D-11-0249.1

61. B. J. Murray, D. O'Sullivan, J. D. Atkinson, M. E. Webb, Ice nucleation by particles immersed in supercooled cloud droplets. *Chem. Soc. Rev.* **41**, 6519 (2012). doi:10.1039/c2cs35200a Medline

62. P. J. DeMott, An exploratory study of ice nucleation by soot aerosols. *J. Appl. Meteorol.* **29**, 1072 (1990). doi:10.1175/1520-0450(1990)029<1072:AESOIN>2.0.CO;2

63. R. Iannone, D. I. Chernoff, A. Pringle, S. T. Martin, A. K. Bertram, The ice nucleation ability of one of the most abundant types of fungal spores found in the atmosphere. *Atmos. Chem. Phys.* **11**, 1191 (2011). doi:10.5194/acp-11-1191-2011

64. L. R. Maki, K. J. Willoughby, Bacteria as biogenic sources of freezing nuclei. *J. Appl. Meteorol.* **17**, 1049 (1978). doi:10.1175/1520-0450(1978)017<1049:BABSOF>2.0.CO;2

65. K. Jayaweera, P. Flanagan, Investigations on biogenic ice nuclei in the Arctic atmosphere. *Geophys. Res. Lett.* **9**, 94 (1982). doi:10.1029/GL009i001p00094

66. O. Möhler *et al*., Heterogeneous ice nucleation activity of bacteria: New laboratory experiments at simulated cloud conditions. *Biogeosciences* **5**, 1425 (2008). doi:10.5194/bg-5-1425-2008

67. E. Attard *et al*., Effects of atmospheric conditions on ice nucleation activity of Pseudomonas. *Atmos. Chem. Phys.* **12**, 10667 (2012). doi:10.5194/acp-12-10667-2012

68. O. Möhler *et al*., Effect of sulfuric acid coating on heterogeneous ice nucleation by soot aerosol particles. *J. Geophys. Res.* **110**, D11210 (2005). doi:10.1029/2004JD005169

69. Z. A. Kanji, P. J. DeMott, O. Möhler, J. P. D. Abbatt, Results from the University of Toronto continuous flow diffusion chamber at ICIS 2007: Instrument intercomparison and ice onsets for different aerosol types. *Atmos. Chem. Phys.* **11**, 31 (2011). doi:10.5194/acp-11-31-2011

70. I. Crawford *et al*., Studies of propane flame soot acting as heterogeneous ice nuclei in conjunction with single particle soot photometer measurements. *Atmos. Chem. Phys.* **11**, 9549 (2011). doi:10.5194/acp-11-9549-2011

71. K. A. Koehler *et al*., Cloud condensation nuclei and ice nucleation activity of hydrophobic and hydrophilic soot particles. *Phys. Chem. Chem. Phys.* **11**, 7906 (2009). doi:10.1039/b905334b Medline